

Perturbation theory and excursion set estimates of the probability distribution function of dark matter, and a method for reconstructing the initial distribution function

Tsz Yan Lam^{*} & Ravi K. Sheth^{*}

Department of Physics & Astronomy, University of Pennsylvania, 209 S. 33rd Street, Philadelphia, PA 19104, USA

27 October 2018

ABSTRACT

Nonlinear evolution is sometimes modeled by assuming there is a deterministic mapping from initial to final values of the locally smoothed overdensity. However, if an underdense region is embedded in a denser one, then it is possible that its evolution is determined by its surroundings, so the mapping between initial and final overdensities is not as ‘local’ as one might have assumed. If this source of nonlocality is not accounted for, then it appears as stochasticity in the mapping between initial and final densities. Perturbation theory methods ignore this ‘cloud-in-cloud’ effect, whereas methods based on the excursion set approach do account for it; as a result, one may expect the two approaches to provide different estimates of the shape of the nonlinear counts in cells distribution. We show that, on scales where the rms fluctuation is small, this source of nonlocality has only a small effect, so the predictions of the two approaches differ only on the small scales on which perturbation theory is no longer expected to be valid anyway. We illustrate our results by comparing the predictions of these approaches when the initial-final mapping is given by the spherical collapse model. Both are in reasonably good agreement with measurements in numerical simulations on scales where the rms fluctuation is of order unity or smaller.

If the deterministic mapping from initial conditions to final density depends on quantities other than the initial density, then this will also manifest as stochasticity in the mapping from initial density to final. For example, the Zeldovich approximation and the Ellipsoidal Collapse model both assume that the initial shear field plays an important role in determining the evolution. We compare the predictions of these approximations with simulations, both before and after accounting for the ‘cloud-in-cloud’ effect. Our analysis accounts approximately for the fact that the shape of a cell at the present time is different from its initial shape; ignoring this makes a noticeable difference on scales where the rms fluctuation in a cell is of order unity or larger.

On scales where the rms fluctuation is 2 or less, methods based on the spherical model are sufficiently accurate to permit a rather accurate reconstruction of the shape of the initial distribution from the nonlinear one. This can be used as the basis for a method for constraining the statistical properties of the initial fluctuation field from the present day field, under the hypothesis that the evolution was purely gravitational. We illustrate by showing how the highly non-Gaussian nonlinear density field in a numerical simulation can be transformed to provide an accurate estimate of the initial Gaussian distribution from which it evolved.

Key words: methods: analytical - dark matter - large scale structure of the universe

1 INTRODUCTION

The present work is primarily concerned with the probability distribution function (hereafter pdf; some authors

prefer to call this the probability density function), which describes the probability that a randomly placed cell of specified shape and volume contains a certain amount of mass. In the best studied cosmological models, the pdf has a Gaussian form initially, but becomes increasingly positively skewed at later times. There are two methods

^{*} E-mail: tylam@sas.upenn.edu, shethrk@physics.upenn.edu

for estimating the evolution of the dark matter pdf. One is based on perturbation theory (Bernardeau 1994; Protogeros & Scherrer 1997; Gaztañaga & Croft 1999; Scherrer & Gaztañaga 2001; Bernardeau et al. 2002) and the other is based on excursion set methods (Sheth 1998). The perturbation theory based calculation is not expected to be accurate on scales where the variance is of order unity or larger; in hierarchical models, this means that perturbation theory is not expected to be accurate on small scales. Hyperextended Perturbation Theory (HEPT) (Scoccimarro & Frieman 1999) is expected to be valid in the larger variance (small cell) regime where standard perturbation theory breaks down; it provides explicit expressions for the moments of the pdf rather than a closed form expression. For the special case of clustering from white-noise Gaussian initial conditions, the excursion set method predicts exactly the same pdf as does HEPT, despite the fact that the methods used by the two approaches are very different. Motivated by this coincidence, the purpose of the present note is twofold: first, to show that, for more general initial conditions, the excursion set approach actually makes rather similar predictions to those of perturbation theory on scales where the variance is small; the second is to understand why.

In the analysis which follows, we distinguish between two steps in the calculation of the pdf. The first is the approximation for nonlinear evolution which we will call the dynamics. The second is how this approximation is used to translate from the initial pdf to an evolved one, which we call the statistics. In the first half of this paper, we study approximations for the dynamics which are based on the assumption of spherical symmetry. In this case, the perturbation theory method provides what is, in effect, a monotonic, deterministic mapping between the initial and final overdensities. Because the final overdensity at a specified position in space is determined solely by the initial value at that position, this is sometimes also called a ‘local’ mapping, since values of the initial fluctuation field at other positions are assumed to not affect the mapping.

The excursion set approach accounts for the fact that the evolution of a given region may actually be determined by less local surroundings. For example, consider the evolution of an underdense region which is surrounded by a dense shell. If the shell is sufficiently dense, then it will eventually collapse, crushing the smaller region within it. The local approximation would have predicted expansion rather than collapse for the smaller underdense region. Sheth & van de Weygaert (2004) call this the void-in-cloud problem, although it is clear that this is an extreme example of a more general ‘cloud-in-cloud’ problem. Clearly, in such cases, the mapping between initial and final overdensities is not as ‘local’ as perturbation theory assumes, and accounting for this ‘cloud-in-cloud’ problem is likely to be more important for small ‘clouds’. If not accounted for, this effect will manifest both as stochasticity (since the same initial overdensity may map to many different final densities depending on the surroundings) and, perhaps, as a bias. The excursion set approach provides an algorithm which accounts for this source of non-locality; it assumes that, once the correct large scale has been chosen, the mapping is deterministic.

However, there is another source of non-locality which spherical evolution models ignore. This source plays a cru-

cial role in models which account for the influence of the external shear field on the evolution. The simplest of these more sophisticated models for the dynamics is the Zeldovich approximation (Zeldovich 1970). Here, the nonlinear density is determined not just by the initial overdensity, but by two other quantities which are related to the surrounding shear field. These quantities also play an important role in extensions of the Zeldovich approximation (Makler et al. 2001) as well as in ellipsoidal collapse models (White & Silk 1979; Bond & Myers 1996). In all these models, the nonlinear density is a deterministic function of three quantities associated with the initial fluctuation field. In the context of perturbation theory models for the pdf, the mapping from initial density to final density will appear to be stochastic if the influence of the two other variables is not accounted for. In the excursion set approach, this stochasticity is in addition to that which derives from the cloud-in-cloud problem which is now associated with all three variables.

To explore the consequences of this additional source of stochasticity we show the result of inserting the Ellipsoidal collapse model into the perturbation theory and excursion set calculations. We do this in two steps: by showing the predictions when expanding the dynamics to first, and then to second order. To first order, the Ellipsoidal collapse model reduces to the Zeldovich approximation; hence, our perturbation theory discussion of the first order approximation extends previous work on the Zeldovich approximation (Kofman et al. 1994; Hui, Kofman & Shandarin 2000). However, our analysis also accounts for another subtlety associated with non-spherical collapse models—that the final shape of a patch is different from its initial shape (Betancort-Rijo 1991; Padmanabhan & Subramanian 1993; Betancort-Rijo & Lopez-Corredoira 2002). We then present the results of the simplest excursion set treatment of this problem which accounts for the evolution in the volumes but not the shapes of cells.

The perturbation theory and excursion set predictions associated with spherical dynamics are presented in Section 2. This section also contains a discussion of the Log-normal model. It includes a comparison of these predictions with measurements in simulations. The perturbation and excursion set treatments of the Zeldovich and ellipsoidal collapse models are in Section 3. A final section summarizes our findings, and includes a discussion of the fact that local deterministic mapping models of nonlinear evolution motivate a simple method for reconstructing the shape of the initial pdf from that at late times. We illustrate the method using the spherical evolution model; we also show that, for the present purposes, the spherical model is a good enough approximation to the second order ellipsoidal collapse dynamics.

2 DETERMINISTIC MAPPINGS FROM INITIAL TO FINAL DENSITY

This section describes the perturbation theory and excursion set models of the pdf when the mapping from linear to nonlinear density is deterministic. In both, the variance of the initial density fluctuation field when smoothed on scale

R_M plays an important role. It is denoted by

$$\sigma_L^2(M) \equiv \int \frac{dk}{k} \frac{k^3 P_L(k)}{2\pi^2} |W(kR_M)|^2 \quad (1)$$

where $P_L(k)$ is the power spectrum of the initial field, $W(x)$ is the Fourier transform of the smoothing window, and $R_M \equiv (3M/4\pi\bar{\rho})^{1/3}$. We will also use the quantity

$$\gamma \equiv -3 \frac{d \ln \sigma_L^2}{d \ln M}. \quad (2)$$

For $P(k) \propto k^n$, $\gamma = (n+3)$.

2.1 Perturbation theory-based methods

These methods make three important assumptions. First, an initial overdensity δ_L can be mapped to an evolved density ρ . Because ρ at any given position in space is determined from δ_L at the same position (in Lagrangian coordinate), the mapping is said to be ‘local’. Because ρ depends on δ_L and nothing else, the mapping is said to be ‘deterministic’. Notice that these ‘local’ ‘deterministic’ assumptions make no mention of the scale on which they apply. In what follows, we will write the evolved density in a cell of volume V , in units of the background density, as

$$\rho \equiv \frac{M}{\rho_b V} \equiv 1 + \delta; \quad (3)$$

we hope that this slight abuse of notation will not cause confusion. Since the evolved density is clearly smoothed on scale V , the question is: on what smoothing scale should the initial overdensity δ_L associated with ρ be defined? This is where the third key assumption is made: the appropriate scale is that which initially contains mass M . As a result of this assumption, the cumulative distributions of the evolved (Eulerian) pdf at fixed V and the initial (Lagrangian) pdf at fixed mass scale M are related as follows (see Section 5.4.3 in Bernardeau et al. 2002):

$$\int_M^\infty dM p(M|V) \frac{M}{\bar{M}} = \int_{\delta_L(M|V)/\sigma_L(M)}^\infty dx \frac{\exp(-x^2/2)}{\sqrt{2\pi}}, \quad (4)$$

where $\bar{M} \equiv \int_0^\infty dM p(M|V) M$, σ_L is given by equation (1), and the right hand side assumes that the initial distribution was Gaussian. Differentiating with respect to M yields

$$\frac{M}{\bar{M}} p(M|V) = \frac{\exp[-(\delta_L/\sigma_L)^2/2]}{\sqrt{2\pi}} \frac{d(\delta_L/\sigma_L)}{dM}. \quad (5)$$

Since $M/\bar{M} \equiv \rho$, the expression above implies that

$$\rho^2 p(\rho|V) = \exp\left[-\frac{\delta_L^2}{2\sigma_L^2}\right] \sqrt{\frac{\delta_L^2}{2\pi\sigma_L^2}} \frac{d \ln(\delta_L/\sigma_L)}{d \ln \rho}. \quad (6)$$

The requirement that the left hand side of equation (4) decreases monotonically with increasing M (since we want $p(M|V) \geq 0$ for all M) means that δ_L/σ_L must increase monotonically with increasing M . As a result, the range of allowed $\delta_L(M|V)$ relations is constrained by the relation $\sigma_L(M)$, i.e., by the initial power spectrum.

2.2 Excursion set method

The excursion set model (Sheth 1998) exploits the fact that $\sigma_L^2(M)$ is a monotonic function of M , so the local collapse

model $\delta_L(M|V)$ defines a curve in the space of δ_L versus σ_L^2 . In what follows, we will set $S(M) = \sigma_L^2(M)$. Then, the excursion set model for the distribution of M in cells of size V is

$$\rho^2 p(\rho|V) = S f(S|V) \frac{d \ln S}{d \ln \rho} \quad (7)$$

where $f(S|V) dS$ denotes the probability that a random walk with uncorrelated steps first crosses a barrier of height $B(S|V)$ on scale S (where S denotes the variance in walk heights). The collapse dynamics is included in this solution of the statistical problem by setting $B(S|V) = \delta_L(\sigma_L^2)$. It is by relating the counts in cells distribution to the first crossing distribution that the excursion set model accounts for the ‘cloud-in-cloud’ problem discussed in the Introduction. Note that this method allows a larger range of $\delta_L(M|V)$ relations than does perturbation theory.

We have used two methods for computing $f(S|V) dS$: one is a Monte-Carlo approach, where we simulate a large ensemble of random walks and count the distribution of first crossings, and the other is the analytical approximation of Sheth & Tormen (2002). This approximation sets

$$f(S|V) dS = |T(S|V)| \exp\left[-\frac{B(S|V)^2}{2S}\right] \frac{dS/S}{\sqrt{2\pi S}}, \quad (8)$$

where $T(S|V)$ denotes the first few terms of the Taylor expansion of B about S . For the barrier shapes of interest in this paper, including only the first two terms is sufficient, so

$$T(S|V) \approx B(S|V) \left[1 - \frac{\partial \ln B(S|V)}{\partial \ln S}\right], \quad (9)$$

where the derivative is evaluated at S . Thus,

$$\begin{aligned} \rho^2 p(\rho|V) &= \exp\left[-\frac{B(S|V)^2}{2S}\right] \sqrt{\frac{B(S|V)^2}{2\pi S}} \frac{d \ln S}{d \ln \rho} \\ &\times \left|1 - \frac{\partial \ln B(S|V)}{\partial \ln S}\right| \\ &= \exp\left[-\frac{\delta_L^2}{2\sigma_L^2}\right] \sqrt{\frac{\delta_L^2}{2\pi\sigma_L^2}} \left|\frac{d \ln(\delta_L/\sigma_L^2)}{d \ln \rho}\right|, \end{aligned} \quad (10)$$

where the final expression uses the fact that $B^2/S \equiv (\delta_L/\sigma_L)^2$. Comparison with perturbation theory (equation 6) shows that the only difference is in the Jacobian like term, which differs by a factor of σ_L .

2.3 Normalization

Direct implementation of the two methods described above produces distributions which are guaranteed to have the correct mean value, $\int d\rho p(\rho|V) \rho = 1$, but, in general, $\int d\rho p(\rho|V) \neq 1$. (Strictly speaking, the analytic approximation to the random walk does not integrate to unity; the Monte-Carlo solution, of course, does; nevertheless the analytical formula gives a very good approximation.) To ensure that this integral also equals unity, one must define

$$N \equiv \int_0^\infty d\rho p(\rho), \quad \rho' \equiv N\rho, \quad \text{and} \quad \rho'^2 p'(\rho') = \rho^2 p(\rho). \quad (11)$$

The quantities ρ' and $p'(\rho')$ now satisfy both normalisation requirements: $\int d\rho' p'(\rho') = 1$ and $\int d\rho' p'(\rho') \rho' = 1$. Note that although this procedure is standard (Kofman et al. 1994; Protoeros & Scherrer 1997;

Ohta et al. 2004), this procedure has no physical motivation, other than to insure correct normalization.

The last of the expressions above shows that plots of $\rho^2 p(\rho)$ versus $\log(\rho)$ can be turned into properly normalized plots simply by shifting along the $\log(\rho)$ direction. This is useful because, as equations (6) and (7) show, it is $\rho^2 p(\rho)$ which is the fundamental prediction of both models for the statistics. We will use this in what follows.

2.4 Example: The Lognormal distribution

The standard form of the Lognormal distribution is

$$\rho^2 p(\rho) = \frac{\exp[-(\ln \rho + \mu)^2 / 2\sigma^2]}{\sqrt{2\pi}} \frac{\rho}{\sigma} \quad (12)$$

where $\mu = \sigma^2/2$ and $\sigma^2 = \ln\langle\rho^2\rangle$. This can be scaled to a Gaussian distribution in the variable δ_L with mean zero and variance σ_L by setting $\rho \equiv 1 + \delta \propto \exp(\delta_L)$ so $\ln(1 + \delta) \propto \delta_L$ where the constant of proportionality is set by requiring that $\langle\rho\rangle = 1$.

However, if one views the transformation $\rho \propto \exp(\delta_L)$ as a local deterministic mapping between the initial overdensity δ_L and evolved density ρ (see Coles & Jones 1991 and Smith, Scoccimarro & Sheth 2007 for motivation), then equation (12) is *not* the form which one obtains from the perturbation theory-like argument we have just described. In this context, equation (12) corresponds to the Lagrangian rather than Eulerian space pdf. This curious fact does not appear to have received attention before. The distinction is important, because, for most power spectra of current interest, $\delta_L(M|V)/\sigma_L(M) \propto \ln(M/V)/\sigma_L(M)$ is not monotonic in M , so the method of Section 2.1 breaks.

2.5 Example: Spherical collapse dynamics

The spherical collapse model relates δ_L and ρ ; it is well approximated by

$$1 + \delta_{NL} \equiv \rho = \left(1 - \frac{\delta_L}{\delta_c}\right)^{-\delta_c} \quad (13)$$

(Bernardeau 1994). The exact value of δ_c depends on the background cosmology. It is $\delta_c \approx 1.686$ in an Einstein de-Sitter model, and $\delta_c \approx 1.66$ for the simulation results we present later. As a result, setting $\delta_c = 5/3$ is an excellent approximation which we will use to provide simple analytic examples of our results. Note that the model studied by Sheth (1998) was, in effect, $\delta_c = 1$; for white-noise initial conditions (initial spectral slope $n = 0$), the resulting excursion set prediction is in exact agreement with HEPT. As we discuss in more detail later, this expression with $\delta_{sc} = 3$ is what the Zeldovich approximation yields for the collapse of a spherical perturbation.

The perturbation theory prediction for the pdf associated with the spherical collapse mapping (equation 13) is

$$\rho^2 p(\rho|V) = \frac{1}{\sqrt{2\pi\sigma_L^2(\rho)}} \exp\left[-\frac{\delta_L^2(\rho)}{2\sigma_L^2(\rho)}\right] \times \left(1 - \frac{\delta_L(\rho)}{\delta_c} + \frac{\gamma}{6}\delta_L(\rho)\right). \quad (14)$$

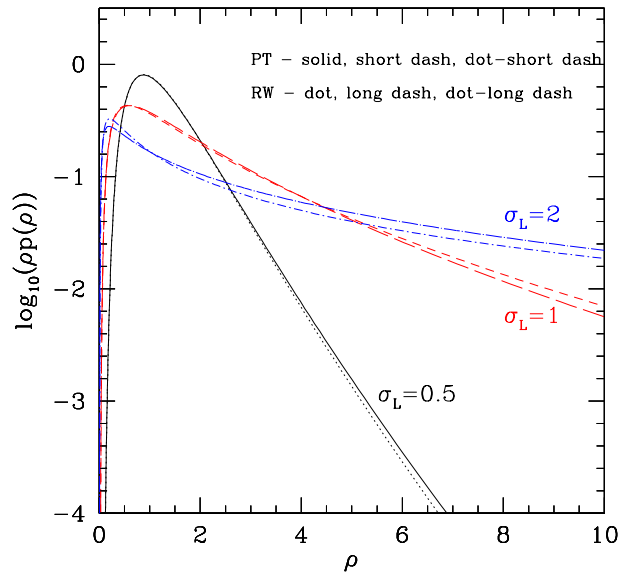


Figure 1. Comparison of equation (A5) (solid, short-dashed, dot-short dashed) and equation (A8) (dotted, long-dashed, dot-long dashed) for $\sigma_V = 0.5, 1.0, 2.0$ respectively.

The corresponding excursion set expression is

$$\rho^2 p(\rho|V) = \frac{1}{\sqrt{2\pi\sigma_L^2(\rho)}} \exp\left[-\frac{\delta_L^2(\rho)}{2\sigma_L^2(\rho)}\right] \times \left(1 - \frac{\delta_L(\rho)}{\delta_c} + \frac{\gamma}{3}\delta_L(\rho)\right). \quad (15)$$

Note that this differs from the perturbation theory expression only because it has a factor of $\gamma/3$ rather than $\gamma/6$. For $|\delta_L(\rho)| \ll 1$, or for $\gamma \ll 6/\delta_{sc} \approx 18/5$, this difference is negligible, and the two models will give very similar results. Demonstrating this agreement between the two methods is one of the central results of this paper.

To illustrate the similarity, and to get a feel for the magnitude of the differences, Figure 1 shows the nonlinear pdf predicted by these models when $\delta_c = 5/3$ and the initial power spectrum was $P(k) \propto k^{-6/5}$. The three sets of curves are for $\sigma_V = 1/2, 1, \text{ and } 2$ (narrowest to broadest distributions).

2.6 Comparison with simulations

We compare our predictions with measurements made in the Very Large Simulation (VLS) (Yoshida et al. 2001). The simulation box represents a cube $479h^{-1}$ Mpc on a side in a cosmological model where $(\Omega_m, \Omega_\Lambda, h, \sigma_8) = (0.3, 0.7, 0.7, 0.9)$. It contains 512^3 particles, so the associated particle mass is $6.86 \times 10^{10} h^{-1} M_\odot$.

We initially counted particles in cubic cells of side $(479/37) h^{-1}$ Mpc; the volume of each cell is equivalent to that of a sphere of radius $8.03 h^{-1}$ Mpc. In the results which follow, counts in larger cells were obtained by summing up counts in neighbouring cells. For cells near the boundary of

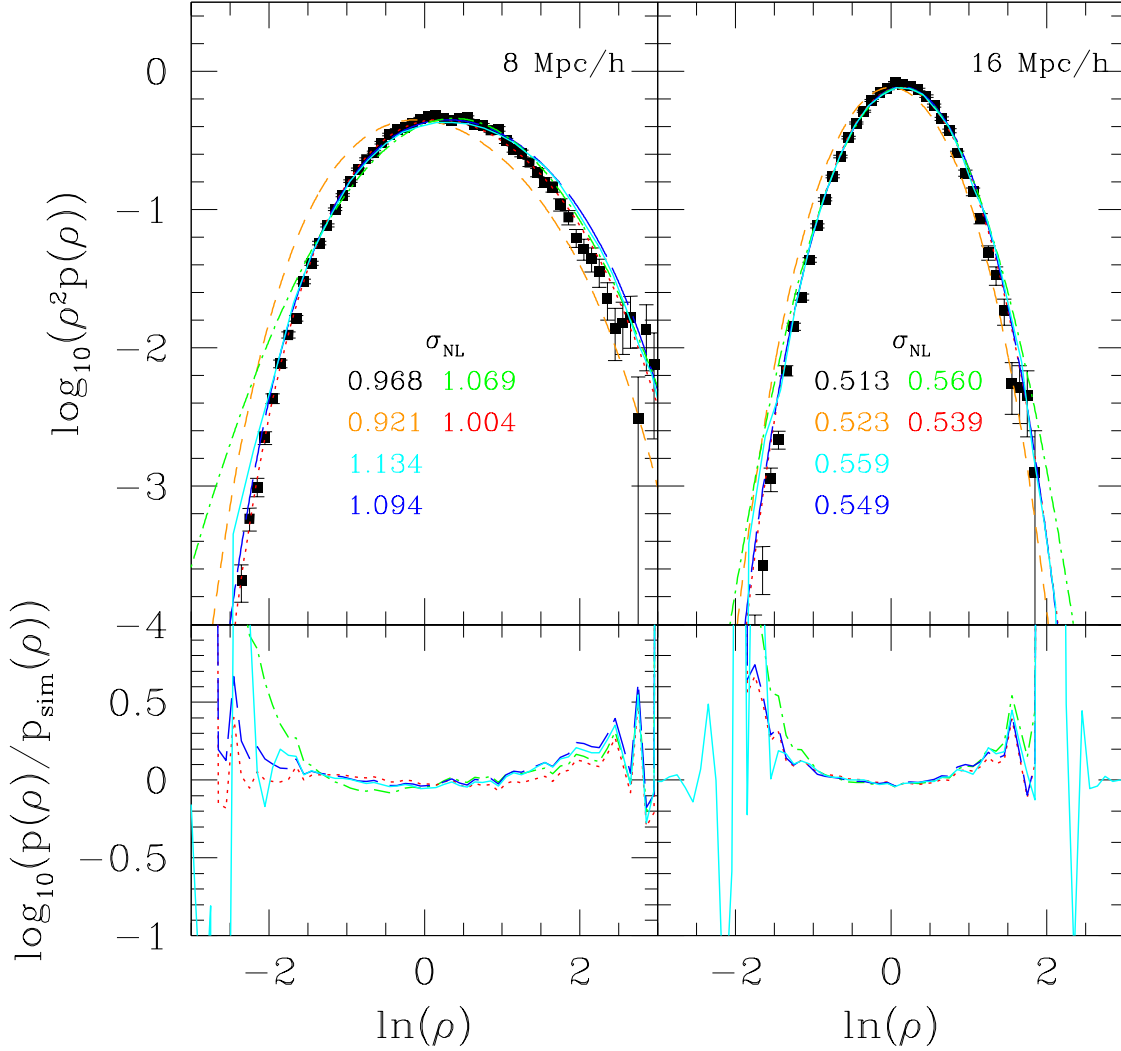


Figure 2. Comparison of the measured $\rho^2 p(\rho)$ (filled squares) with various spherical collapse based predictions for this quantity. Top: dot-dashed (green) curves show the standard Lognormal (equation 12). Short-dashed (orange) and dotted (red) curves show perturbation theory before (equation 14) and after the normalization discussed in Section 2.3 (the dotted curve is simply shifted slightly to the right); solid (cyan) curves show the exact Monte-Carlo solution of the excursion set model, and long-dashed (blue) curves show the associated analytic approximation (equation 15). The nonlinear rms fluctuations of different models are shown in the following order: the VLS simulation (0.968 and 0.513), the Lognormal (1.069 and 0.560), the perturbation theory before normalization (0.921 and 0.523), the perturbation theory after normalization (1.004 and 0.539), the exact Monte-Carlo solution of the excursion set model (1.134 and 0.559), and the analytic approximation (1.094 and 0.549); Bottom: the normalized distributions and the Lognormal divided by the measurements.

the box, we used the fact that the simulation was run using periodic boundary conditions.

Because one does not simulate the nonlinear evolution of a continuous density field, rather, one simulates the motion of particles, the relation between the discrete particle pdf one measures in simulations is non-trivial. Typically, one assumes that the distribution of particle counts in cells is

$$p(N|V) = \int dM p(M|V) p(N|M), \quad (16)$$

where $p(N|M)$ denotes the probability that a mass M

is represented by N particles. If m denotes the particle mass, then the Poisson model assumes that $p(N|M) = (M/m)^N \exp(-M/m)/N!$. Our comparisons with the theoretical models of the previous section assume that discreteness effects are negligible, so $N/\bar{N} = M/\bar{M}$.

The top panel of Figure 2 shows the pdf of the dark matter in cells of two different volumes (equivalent to spheres of radii 8 and 16 h^{-1} Mpc), chosen to have rms fluctuation values of unity or less. Black squares show the measurements in the VLS, where $\rho \equiv 1 + \delta_{\text{NL}} = N/\bar{N}$. Curves show the predictions of the different models: the Lognormal is dot-dashed

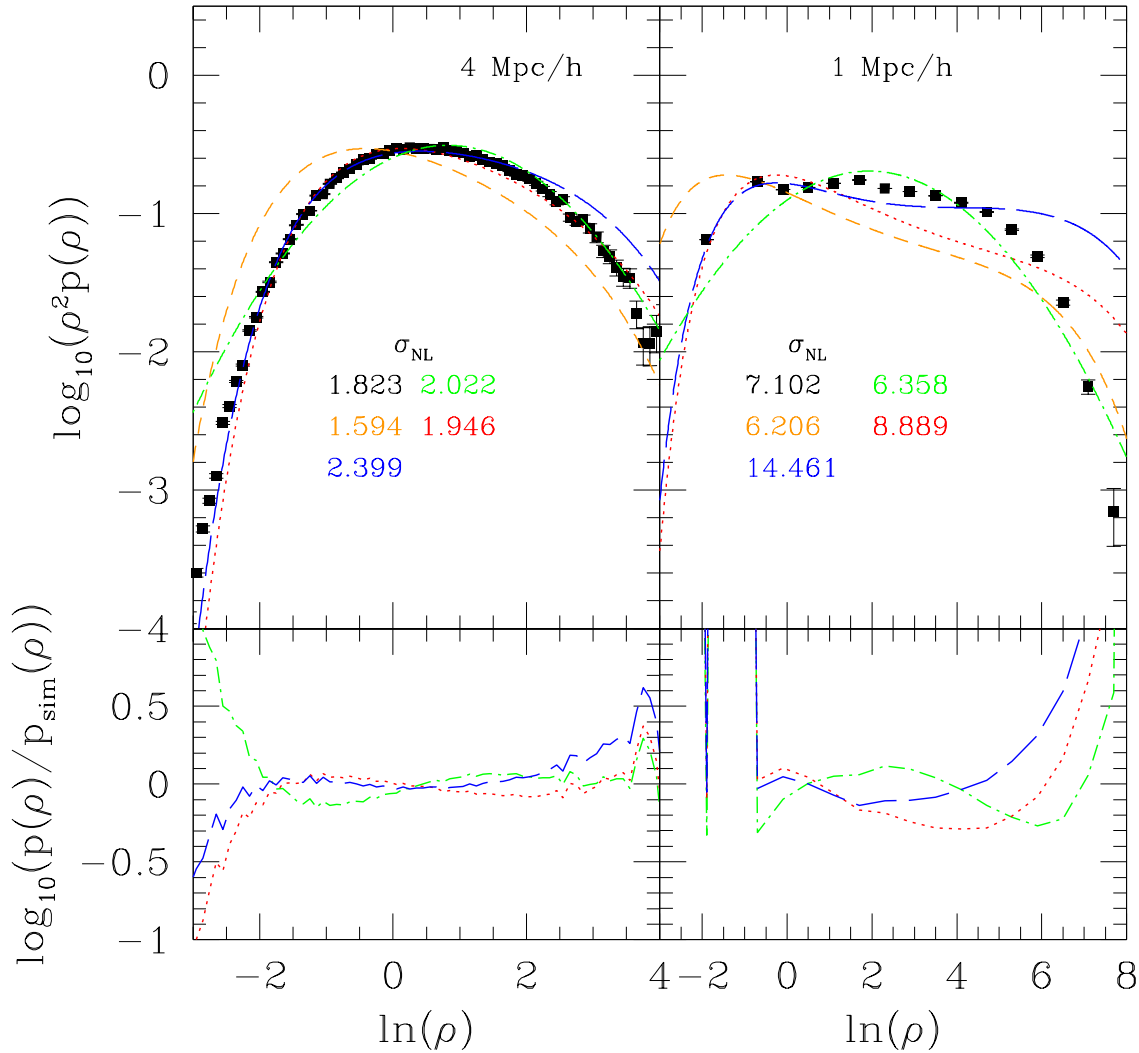


Figure 3. Same as previous figure, but for smaller cells, in which the rms fluctuation is significantly larger than unity. The results from the exact Monte-Carlo solution of the excursion set model are not included as the associated analytical approximation gives very similar results.

(this model has one free parameter, the nonlinear variance, which we compute from the fitting formula in Smith et al. (2003), rather than using the value measured in the simulations); raw and normalized perturbation theory model are short-dashed and dotted (note that the normalised curve is simply shifted to the right of the unnormalised curves); and the excursion set model is solid (long-dashed curve shows the analytic approximation). The nonlinear variances σ associated with these various models are also shown (from left to right, top to bottom: VLS simulation, lognormal, unnormalised perturbation theory, normalised perturbation theory, excursion set from Monte-Carlo, and excursion set from the approximation formula).

To reduce the dynamic range, the bottom panel shows the predictions and Lognormal all ratioed to the measurements. This shows clearly that both the normalised pertur-

bation theory and excursion set models are in better agreement with the simulations than is the Lognormal. We note in passing that Betancort-Rijo & Lopez-Corredoira (2002) provide a relatively simple analytic expression for the nonlinear pdf. Their expression is, essentially, yet another prediction for the spherical evolution based pdf. It fares substantially worse than either of our models - it overpredicts the high density tail - so we do not show it here.

Figure 3 shows that these spherical collapse based predictions remain accurate even on scales where the rms fluctuation is significantly larger than unity. This is well beyond the regime where standard perturbation theory is expected to be valid, and indeed, the perturbation and excursion set predictions for the high density tails differ significantly. Perturbation theory provides a substantially better description of the simulations when the rms fluctuation is of order 2 (left

panel) but is worse when the rms is larger (right panel). On the other hand, the average density within the virial radius of a dark matter halo is about 200 times the background density; thus, in the regime where $\ln \rho \geq 5$, the mapping of equation (13) is suspect.

Figures 2 and 3 show that the spherical model produces rather accurate predictions for the shape of the nonlinear pdf, at least on scales where the nonlinear rms fluctuation is smaller than about 2. We show later that this can be used to motivate an algorithm which uses the nonlinear density field to provide an estimate of the initial pdf.

3 STOCHASTIC MAPPINGS FROM INITIAL TO FINAL DENSITY

In this section we replace the assumption of a spherical collapse in favor of the ellipsoidal collapse model. This evolution is considerably more complex, and so we only present results to first and second order in the dynamics. We use the formulation of this model in which it reduces, to lowest order, to the Zeldovich Approximation (Bond & Myers 1996).

3.1 The Zeldovich Approximation

In the Zeldovich Approximation, the nonlinear density is a deterministic function of three numbers in the initial distribution. These are the eigenvalues λ_i of the deformation tensor, a 3×3 symmetric matrix whose elements are the second derivatives of the initial potential field.

The initial density δ_L is the sum of the three eigenvalues, whereas the nonlinear density is

$$\rho = \prod_{i=1}^3 (1 - \lambda_i)^{-1}. \quad (17)$$

(note that $\rho \rightarrow 1 + \sum_i \lambda_i$ when $\lambda \ll 1$). All three eigenvalues are the same for a sphere, in which case $\lambda = \delta_L/3$. In this case, the relation above reduces to that of the spherical model from the previous section with $\delta_c = 3$. Similarly, $\delta_c = 2$ is associated with regions where the smallest eigenvalue is zero, and the other two are each equal to $\delta_L/2$. If one calls such an object a filament, then a sheet has two eigenvalues equal to zero and the third equal to δ_L , so the evolution is given by equation (13) with $\delta_c = 1$.

The evolved pdf of this model has

$$\rho p(\rho|V) d\rho = \int d\lambda p(\lambda|\sigma) \delta_D \left(\rho = \prod_{i=1}^3 (1 - \lambda_i)^{-1} \right) \quad (18)$$

(Padmanabhan & Subramanian 1993; Hui, Kofman & Shandarin 2000; Betancort-Rijo & Lopez-Corredoira 2002).

For Gaussian initial conditions, the joint distribution of $p(\lambda_1, \lambda_2, \lambda_3|\sigma)$ is known (Doroshkevich 1970), and it is straightforward to evaluate the integral above by Monte Carlo methods. In practice, this distribution is a function of λ_i/σ , so it is useful to think of the expression above as

$$\rho p(\rho|V) d\rho = \int d\lambda p(\lambda|1) \delta_D \left(\rho = \prod_{i=1}^3 (1 - \sigma \lambda_i)^{-1} \right). \quad (19)$$

Notice that if $\sigma = \sigma_L(\bar{\rho}V) \equiv \sigma_V$, then

$$\int p(\rho|V) d\rho = \int d\lambda p(\lambda|1) \prod_{i=1}^3 (1 - \sigma_V \lambda_i) = 1. \quad (20)$$

This choice is made by Hui et al. (2000); in this case, the normalization problems of Section 2.3 do not arise. However, the analysis of the previous sections suggests that this ignores the effects of smoothing, and that setting $\sigma = \sigma_L(M)$ is almost certainly a better choice (Betancort-Rijo 1991; Padmanabhan & Subramanian 1993; Betancort-Rijo & Lopez-Corredoira 2002).

Notice that if any one of the eigenvalues equals unity then the density diverges, and that the density becomes negative if one and only one or all three eigenvalues exceed unity. This happens often when $\sigma \geq 1$ (with probability 11% when $\sigma = 1$), thus restricting the use of this approximation to large scales where σ is small. Accounting for the effects of smoothing will mitigate this somewhat, since $\sigma_M \ll \sigma_V$ when $\rho \gg 1$, where we have defined $\sigma_M \equiv \sigma_L(M)$ and $\sigma_V \equiv \sigma_L(\bar{\rho}V)$. For simplicity, on the few occasions when the density does go negative, we take the absolute value of the *rhs* of equation (17); there is no physical motivation for this choice, but, in practice, this happens sufficiently rarely that it does not affect our results.

The expression above is still not entirely self-consistent. Although it tries to account for the fact that the final size of a region is different from its initial size, it does *not* account for the fact that the shape has also changed (Betancort-Rijo 1991; Padmanabhan & Subramanian 1993; Betancort-Rijo & Lopez-Corredoira 2002). If the final volume V is spherical, the initial volume was not; the analysis above does not account for this. However, this can be done in a relatively straightforward way by simply setting $\sigma_L(\lambda)$, where, for Eulerian spheres V of radius R_E we require that $R_E = R_i(1 - \lambda_i)$. This means that the delta function picks out ellipsoids in the initial field which contained mass $M \propto \prod_{i=1}^3 R_i$, and which are now spheres of volume V which contain the same mass M . The function $\sigma_L(\lambda)$ is the rms fluctuation in the initial field when smoothed with a triaxial filter of shape given by (R_1, R_2, R_3) ; we have checked that it is well approximated by

$$\sigma_L^{\text{Ell}}(\lambda) = \sigma_L^{\text{Sph}}(M) \exp \left\{ -\frac{B}{2} \sum_{i < j} \left[\ln \left(\frac{1 - \lambda_i}{1 - \lambda_j} \right) \right]^2 \right\}, \quad (21)$$

where $B = 0.0486$, and the subscripts *ell* and *sph* stand for ellipsoidal and spherical respectively (Betancort-Rijo & Lopez-Corredoira 2002). This, then, is our perturbation theory based estimate associated with the Zeldovich Approximation.

Figure 4 shows how the shape dependence of the rms fluctuation changes the predicted dark matter pdf. In the top panel the dotted curves are the predictions of perturbation theory using equation (19) with $\sigma_L(M)$ whereas the dashed curves use $\sigma_L(\lambda)$. The difference between these two is significant, meaning the shape dependence is important, in the high density tail ($\ln(\rho) > 1$) of the $8h^{-1}$ Mpc cells. The bottom panel compares the ratios of different models to the measurements. In neither cases does the Zeldovich Approximation agree well with the simulations: the difference is more than a factor of two in low density regions ($\ln(\rho) < -2$ in $8h^{-1}$ Mpc and $\ln(\rho) < -1.5$ in $16h^{-1}$ Mpc).

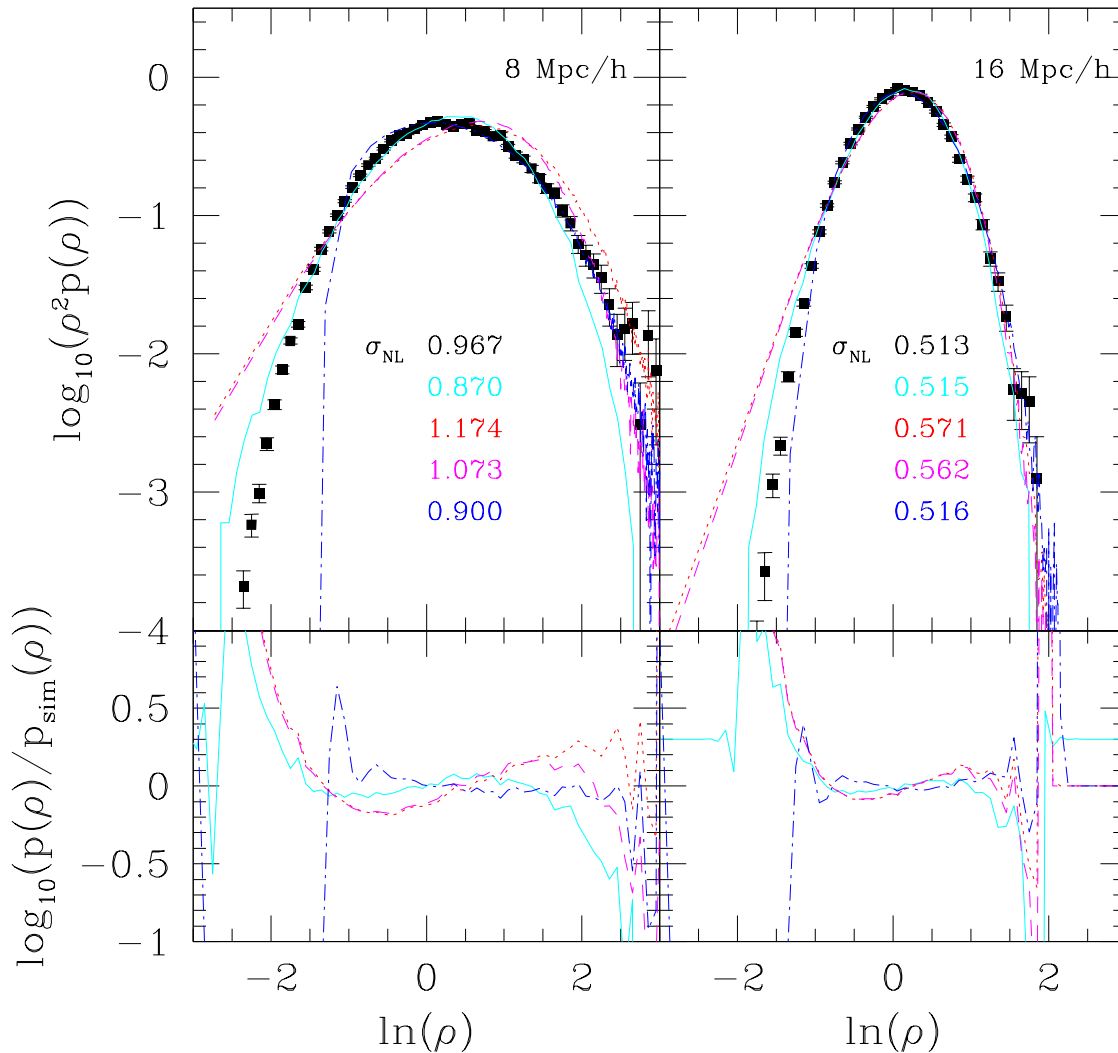


Figure 4. Comparison of the measured $\rho^2 p(\rho)$ (filled squares) and various Zeldovich approximation-based predictions and second order ellipsoidal model using perturbation-theory for this quantity. In the top panel red (dotted) and cyan (solid) curves show the normalized perturbation-theory and excursion-set predictions using the spherical linear variance approximation. Magenta (dash) shows the perturbation-theory prediction using the ellipsoidal variance approximation (equation 21). Blue (dotted-dash) shows the normalized perturbation-theory predictions using second order ellipsoidal collapse model (equation 30). The numbers shown are the rms values for (from top to bottom) VLS simulation, excursion-set (spherical variance), perturbation-theory (spherical variance), perturbation-theory (Zeldovich approximation using ellipsoidal variance), and perturbation-theory (second ellipsoid collapse using ellipsoidal variance). Bottom panel shows the corresponding distributions divided by the measurements.

It is rather more complicated to account approximately for the effect of the change in shape in the excursion set approach. Our Monte Carlo algorithm works as follows. We generate $(\lambda_1, \lambda_2, \lambda_3)$ in each step of the walk following the procedure described by Sheth & Tormen (2002). The variance associated with step n is $S^{(n)}$. This has an associated scale $R^{(n)}$. We are interested in patches which today are spheres of radius R_E . (The extension to ellipsoids at the present time is straightforward). These are those initial patches which satisfy $R_i^{(n)}(1 - \lambda_i^{(n)}) = R_E$, where $\lambda_i^{(n)}$ is the value of λ_i after n steps. We then want the largest mass

associated with the various $R_i^{(n)}$. Since mass is proportional to $\prod_i R_i$, we want the largest value of $R_i^{(n)}$ for each i ; in effect, we want the first crossing values n_i for each of the three barriers $R_i^{(n)}(1 - \lambda_i^{(n)}) = R_E$. Let $f(n_1, n_2, n_3)$ denote the fraction of walks which first cross the three barriers after (n_1, n_2, n_3) steps. Then the excursion set model sets

$$\rho p(\rho|V) d\rho = f(M_{123}) dM_{123}. \quad (22)$$

where

$$M_{123} \propto R_1^{(n_1)} R_2^{(n_2)} R_3^{(n_3)} \quad (23)$$

denotes the mass associated with the first crossing at (n_1, n_2, n_3) . We then renormalize the left hand side following the discussion in Section 2.3. In Figure 4 the cyan (solid) curves show the predictions of the excursion set approach. While they fit better than the perturbation theory's results the agreement is not very good at the low density region.

Although this algorithm allows for different shapes in the initial distribution, it only approximates the exact problem we wish to solve, because the n th step in any given direction is associated with the same value of S_n , whatever the values of n in the other directions. In effect, we are approximating $S(n_1, n_2, n_3)$ with the spherical value S_{n_i} for each axis i .

3.2 The ellipsoidal collapse model

The late time evolution in the ellipsoidal collapse model is more complicated than in the Zeldovich Approximation (Bond & Myers 1996). Nevertheless, we can still write the nonlinear density as a deterministic (albeit complicated) mapping of the three eigenvalues λ in the initial field.

Thus, the non-linear density is given by an expression that is analogous to equation (17). Namely,

$$\rho = \prod_{i=1}^3 (1 - \xi_i)^{-1}, \quad (24)$$

where in an Einstein-de Sitter universe the evolution of ξ_i is described by

$$a^2 \frac{d^2 \xi_i}{da^2} + \frac{3}{2} a \frac{d\xi_i}{da} = \frac{3}{2} (1 - \xi_i) \left(\frac{1}{3} \delta + \frac{1}{2} b_i \delta + L_{\text{ext},i} \right), \quad (25)$$

with

$$b_i = \frac{4}{15} (3\xi_i - \sum_j \xi_j) + O(\xi^2), \quad \text{and} \quad (26)$$

$$L_{\text{ext},i} = \lambda_i - \frac{1}{3} \sum_j \lambda_j \quad (27)$$

This expression for L_{ext} is known as the linear tide approximation (Bond & Myers 1996). The initial condition of equation (25) is the Zeldovich Approximation.

The solution of the differential equation above can be written as a series: $\xi_i = \sum_j \zeta_i^{(j)} a^j$. In what follows we only consider the first two terms in this series:

$$\zeta_i^{(1)} = \lambda_i \quad (28)$$

$$\zeta_i^{(2)} = \frac{3}{50} (I_1^2 - 2I_2) + \frac{11}{175} I_2 + \frac{3}{50} \lambda_i (2I_1 - 5\lambda_i), \quad (29)$$

where $I_1 \equiv \sum_j \lambda_j$ and $I_2 \equiv \sum_{j \neq k} \lambda_j \lambda_k$ (Ohta et al. 2004 provide a similar expansion).

We then apply the same argument as in the previous section for the perturbation-theory approach to calculate the pdf of the evolved density field. Namely, we set

$$\rho p(\rho|V) d\rho = \int d\lambda p(\lambda|1) \delta_D \left(\rho = \prod_{i=1}^3 (1 - \sigma \xi_i)^{-1} \right), \quad (30)$$

where $\sigma \xi_i \equiv \sigma \zeta_i^{(1)} + \sigma^2 \zeta_i^{(2)}$ and σ includes the shape effect (equation 21, with ξ_i values replacing λ_i values).

Figure 5 shows the correlation between the initial and final densities in this model for $8h^{-1}$ Mpc cells. Recall that, because the evolution depends on all three λ_i , whereas the

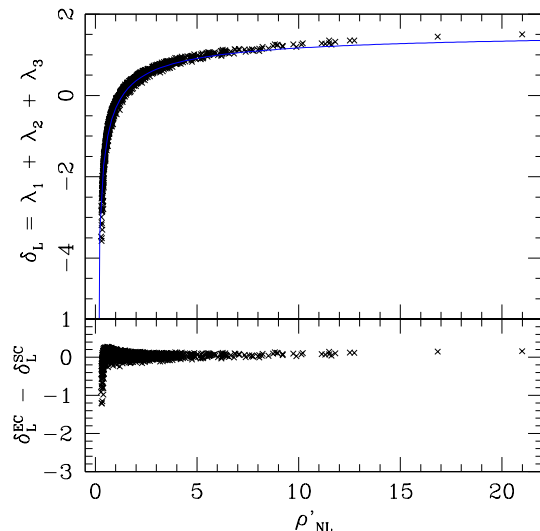


Figure 5. Stochasticity in the mapping between linear and non-linear overdensity on scales of $8h^{-1}$ Mpc. In the upper panel, points show the ellipsoidal collapse mapping associated with equation (30); solid line shows the spherical collapse mapping of equation (13). Both are normalised as described in Section 2.3; $N_{\text{EC}} = 1.087$ for ellipsoidal collapse and $N_{\text{SC}} = 1.33$ for the spherical model. The lower panel shows the difference between these two mappings.

initial density δ_L is simply proportional to $\sum_i \lambda_i$, we expect there to be some stochasticity in ρ at each δ_L . The Figure shows that this is not a very large effect. Moreover, the solid line shows that the spherical collapse mapping (equation 13) provides a reasonably good description of the mean mapping. We exploit this fact in the next section.

The dot-dashed lines in Figure 4 show the predicted pdfs from this second order ellipsoidal collapse model. Note that inclusion of these second order terms provides a clear improvement over the Zeldovich Approximation prediction; this is true over all $\ln(\rho) > -1$ in both the 8 and $16h^{-1}$ Mpc cells. Although the discrepancies at small ρ are the most dramatic (we discuss these in the next section), we are actually more interested in the region around the peak of the pdf: the bottom panels show clearly that the Zeldovich Approximation curves lie snake around the simulation results, whereas this sideways S-shaped residual is largely absent in the second order ellipsoidal collapse model.

4 DISCUSSION

We discussed two approaches (perturbation theory and excursion set) for calculating the dark matter pdf using two different models for the dynamics (spherical collapse and the Zeldovich Approximation) in each case. Although both approaches are deterministic, in the sense that the nonlinear evolution is determined by the initial conditions locally, the excursion set is slightly less ‘local’. We showed that both are expected to give similar predictions whenever the dynamics is approximated by local deterministic mappings (equa-

tion 6), of which the spherical evolution model (equation 13) is a special case (Figure 1). The agreement is important, because the excursion set calculation allows one to connect discussions of the dark matter halo distribution with discussions of the pdf (Sheth 1998).

Both the perturbation and excursion set approaches, when combined with the spherical evolution model, provide good descriptions of the nonlinear pdf seen in simulations (Figures 2 and 3). This agreement is slightly unexpected, in the sense that the spherical evolution model ignores the fact that the nonlinear evolution of a region may be determined by quantities other than its initial density. The ellipsoidal collapse model is a specific example of this; we studied its first (Zeldovich Approximation) and second order expansions in some detail. In this model, the evolution of a patch is determined by its overdensity as well as the surrounding shear field (only the overdensity matters for the spherical collapse model). As a result, nonlinear evolution changes the shape as well as the volume of a patch (in the spherical collapse model, only the volume changes). We found that including the evolution of the shapes is important when the density is high, so this is particularly important when the cell size is small. This shape dependence also complicates the excursion set calculation (Section 3.1).

Despite its increased complexity compared to the spherical evolution model, we found that the Zeldovich Approximation resulted in significantly worse agreement with the simulations (Figure 4). Going to second order in the ellipsoidal collapse model resulted in more accurate predictions, except in the lowest density regions. The relatively large discrepancies in underdense regions, in both models, may be related to the following fact. A Taylor series in δ will converge more rapidly when $\delta > 0$ than when $\delta < 0$, since the latter will be an oscillating series. Thus, it may be that, to accurately represent the evolution of underdense regions, one must go beyond second order in the dynamics. Presumably, going to even higher order would further improve agreement with the simulations; this is the subject of work in progress.

Although our perturbation theory calculation accounts for the evolution of shapes, our excursion set calculation does not. This too is the subject of on-going work. The excursion set calculation is particularly interesting in view of the fact that the marriage of ellipsoidal collapse with the excursion set approach appears to provide a substantially improved prediction of dark halo abundances (Sheth, Mo & Tormen 2001). Finally, we note that our study of the real space pdf can be extended to redshift space; we are in the process of extending previous work on this problem (Protogeros & Scherrer 1997; Hui, Kofman & Shandarin 2000; Ohta et al. 2004).

4.1 An extension

The accuracy of the spherical collapse based predictions, and the fact that the associated deterministic mapping from initial to final overdensity also provides a good description of the mean mapping in the ellipsoidal collapse model (Figure 5), suggests that one might be able to estimate the shape of the initial pdf from a measurement of the evolved one as follows. Starting from equation 13 and the normalization method in section 2.3, there is a mapping from the final density to its initial value. For each measured $M = \bar{\rho}V(1 + \delta_{\text{NL}})$

set

$$\nu = \frac{1 - [(1 + \delta_{\text{NL}})/N_{\text{sc}}]^{-1/\delta_c}}{\sigma_L(M/N_{\text{sc}})/\delta_c}, \quad (31)$$

where δ_c is the critical linear density associated with collapse in the spherical model, and N_{sc} is the corresponding normalization factor (Section 2.3). Then make a histogram of ν , but rather than having each cell count equally, weight each by its value of $(1 + \delta_{\text{NL}})/N_{\text{sc}}$. The resulting distribution of ν should provide a good estimate of the shape of the initial pdf of (δ_L/σ_L) .

Figure 6 shows the results of this algorithm for a number of different scales. Reconstruction of the initial pdf from the nonlinear pdf measured on scales larger than $8h^{-1}\text{Mpc}$ works rather well (top panels). The reconstructed distributions trace the same Gaussian shape very well; for reference, the smooth black curve shows a Gaussian with zero mean and unit variance. This mapping works well even when the cell size is as small as $4h^{-1}\text{Mpc}$ (bottom left), but it fails at $1h^{-1}\text{Mpc}$ (bottom right). The Figure also shows that it is important to account for the factor of $1 + \delta_{\text{NL}}$ which relates Eulerian and Lagrangian statistics: weighting each cell in the nonlinear distribution equally would have lead one to conclude incorrectly that the reconstruction is biased even on very large scales. Studying whether or not this is relevant for the MAK reconstruction method (Mohayaee et al. 2006) is the subject of work in progress.

In effect, the spherical evolution model, when combined with the nonlinear pdf, is able to provide a good description of the initial pdf for scales where the rms fluctuation is smaller than about 2. In principle, this might be used as the basis for a test of the Gaussianity of the initial conditions because the algorithm makes no explicit assumption about the form of the distribution of ν . The fact that the nonlinear pdfs from a range of different scales all map back to the same zero mean, unit variance Gaussian curve suggests that this method is a good test of Gaussianity. Although this is not the first method to reconstruct the shape of the initial one-point density field, it is simple and actually fares rather well compared to a number of previous methods (e.g. Kofman et al. 1994; Narayanan & Croft 1999).

This procedure is not as good a test of non-Gaussianity, in the sense that it does not yield a simple estimate of the shape of the initial distribution if it were non-Gaussian. This is because the reconstruction requires an estimate of the normalization factor N_{sc} , and to calculate it, one must first specify the form of the initial distribution. So the algorithm above is really a self-consistency check: it checks if the assumed form of the initial pdf is consistent with that reconstructed from the measured nonlinear pdf, under the assumption that spherical evolution is a good model whatever the initial fluctuation field. Of course, rescaling to ν involved a rescaling and transformation of the measured M , but it also involved $\sigma(M)$; this is a consequence of the fact that, for Gaussian fluctuations, information about the volume enters only through the scale dependence of the rms value. For more general distributions this may not remain true, in which case the mapping to the initial variable δ_L may be more complicated than equation (31). Nevertheless, Figure 6 suggests that this may be an interesting avenue to explore in future work. We are in the process of extending this method to include redshift space effects, as well as

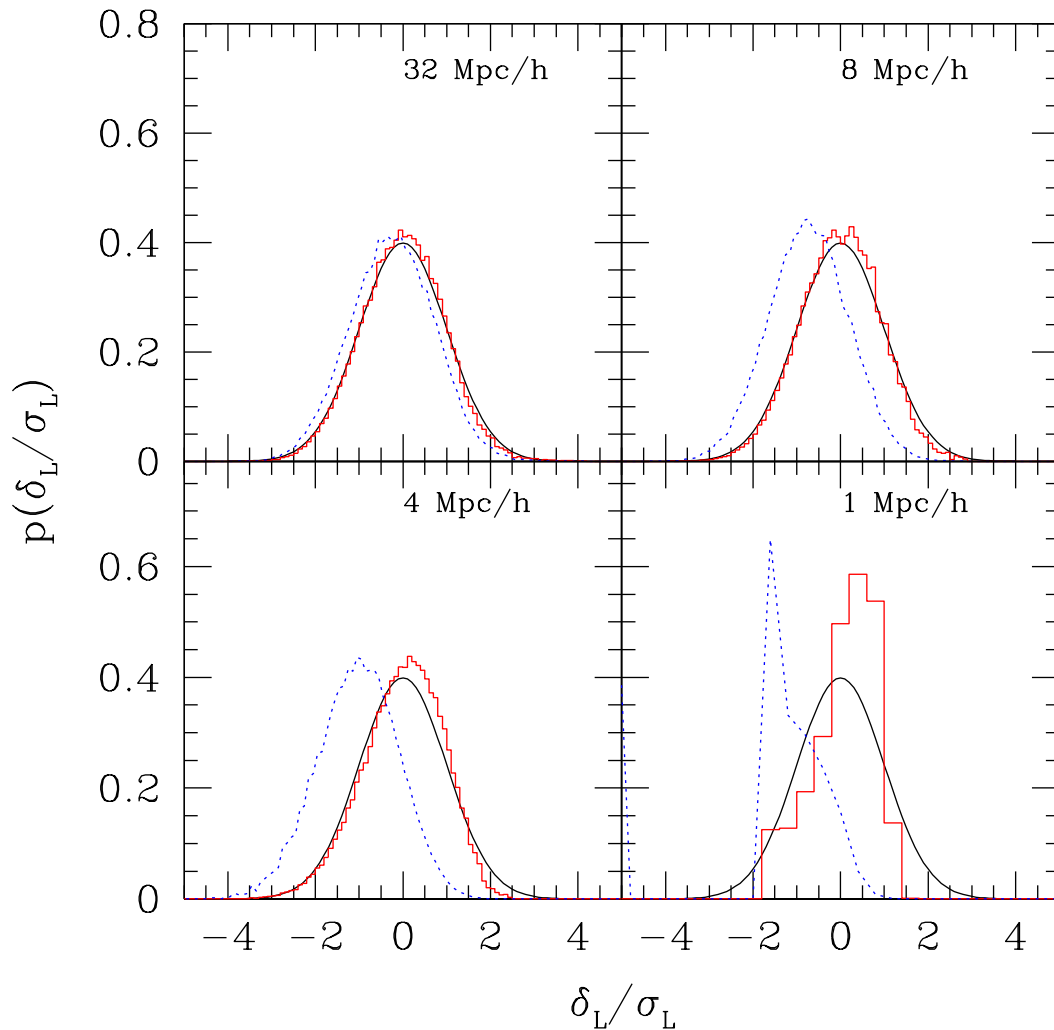


Figure 6. Comparison of the reconstructed linear pdf of δ/σ (histogram) with the expected zero-mean unit-rms Gaussian form (solid line). Different panels show results for reconstructions from different smoothing scales. The method works well for large cells (top panels), but becomes increasingly inaccurate for smaller cells (bottom panels). When the nonlinear rms fluctuation is larger than 2 (bottom right), then the reconstructed pdf is rather different from the Gaussian form, as one might expect from Figure 3. Dotted curves show the bias which results from ignoring the extra weighting factor associated with the transformation from Eulerian to Lagrangian statistics.

galaxy bias. We believe it may be interesting to merge it with the method recently proposed by Eisenstein et al. (2007) for reconstructing the Baryon Acoustic Oscillation feature in the galaxy distribution.

ACKNOWLEDGEMENTS

We thank R. Smith for help with the simulation data, R. Scoccimarro for discussions about stochasticity, E. Gaztañaga for conversations during the NSF-PIRE School held in Santiago, Chile in March 2007, the organizers of the School for inviting us to participate, B. Jain for support, J. Betancort-Rijo for discussions, and the Aspen Center for Physics for its hospitality when some aspects of this work

were completed. We would also like to thank the anonymous referee for a perceptive and helpful report. This work was supported in part by NSF grants 0507501 and 0520677.

REFERENCES

- Bernardeau F., 1994, *A&A*, 291, 697
- Bernardeau F., Colombi S., Gaztañaga E., Scoccimarro R., 2002, *Phys. Rep.* 367, 1
- Betancort-Rijo J., 1991, *MNRAS*, 251, 399
- Betancort-Rijo J., Lopez-Corredoira M., 2002, *ApJ*, 566, 623
- Bond J. R., Myers S. T., 1996, *ApJS*, 103, 1
- Coles P., Jones B. J. T., 1991, *MNRAS*, 248, 1
- Doroshkevich A. G., 1970, *Astrofizika*, 6, 581

Eisenstein D. J., Seo H.-J., Sirko E., Spergel D. N., 2007, ApJ, 664, 675
 Gaztañaga E., Croft R. A. C., 2001, MNRAS, 309, 885
 Hui L., Kofman L., Shandarin S. F., 2000, ApJ, 537, 12
 Kofman L., Bertschinger E., Gelb J. M., Nusser A., Dekel A., 1994, ApJ, 420, 44
 Makler M., Kodama T., Calvão M. O., 2001, ApJ, 557, 88
 Mohayaee R., Mathis H., Colombi S., Silk J., 2006, MNRAS, 365, 939
 Narayanan V. K., Croft R. A., 1999, ApJ, 515, 471
 Ohta Y., Kayo I., Taruya A., 2004, ApJ, 608, 647
 Padmanabhan T., Subramanian K., 1993, ApJ, 410, 482
 Protogeros Z. A. M., Scherrer R. J., 1997, MNRAS, 284, 425
 Scherrer R. J., Gaztañaga E., 2001, MNRAS, 328, 257
 Scoccimarro R., Frieman J., 1999, ApJ, 520, 35
 Sheth R. K., 1998, MNRAS, 300, 1057
 Sheth R. K., Tormen G., 1999, MNRAS, 308, 119
 Sheth R. K., Mo H. J., Tormen G., 2001, MNRAS, 323, 1
 Sheth R. K., Tormen G., 2002, MNRAS, 329, 61
 Sheth R. K., van de Weygaert R., 2004, MNRAS, 350, 517
 Smith R. E., Peacock J. A., Jenkins A., White S. D. M., Frenk C. S., Pearce F. R., Thomas P. A., Efstathiou G., Couchman H. M. P., 2003, MNRAS, 341, 1311
 Smith R. E., Scoccimarro R., Sheth R. K., 2007, PRD, accepted
 White S. D. M., Silk J., 1979, ApJ, 231, 1
 Yoshida N., Sheth R. K., Diaferio A., 2001, MNRAS, 328, 669
 Zeldovich Y. B., 1970, A&A, 5, 84

where

$$N = \frac{10}{3} \frac{e^{25/9\sigma_V^2}}{\sqrt{2\pi}\sigma_V} K_{7/6} \left(\frac{25}{9\sigma_V^2} \right). \quad (\text{A9})$$

In this context, it is interesting that the family of models studied by Sheth (1998) included modified Bessel functions of the third, rather than second, kind. The solid and dotted curves in Figure 1 show equations (A5) and (A8) for a few values of σ_V .

APPENDIX A: FULLY ANALYTIC PDF IN THE SPHERICAL MODEL

For a power-law power spectrum ($P(k) \propto k^n$), the spherical model allows a semi-analytical form of the pdf for some special choices of n . To see this clearly, define $\tilde{\delta}_L$ by

$$\frac{\delta_L(\rho)}{\sigma_V(\rho)} = \frac{1}{\sigma_V} \delta_c \rho^{(n+3)/6} (1 - \rho^{-1/\delta_c}) \equiv \frac{\tilde{\delta}_L(\rho)}{\sigma_V}, \quad (\text{A1})$$

where σ_V is independent of ρ . If we set

$$\frac{n+3}{6} = \frac{1}{2\delta_c}, \quad (\text{A2})$$

then

$$\rho = \left(\frac{\tilde{\delta}_L}{2\delta_c} + \sqrt{\left(\frac{\tilde{\delta}_L}{2\delta_c}\right)^2 + 1} \right)^{2\delta_c} \quad (\text{A3})$$

$$N = \int_{-\infty}^{\infty} d\tilde{\delta}_L \frac{e^{-\tilde{\delta}_L^2/2\sigma_V^2}}{\sqrt{2\pi}\sigma_V} \left(\frac{\tilde{\delta}_L}{2\delta_c} + \sqrt{\left(\frac{\tilde{\delta}_L}{2\delta_c}\right)^2 + 1} \right)^{-2\delta_c} \quad (\text{A4})$$

and the normalised perturbation theory pdf is

$$\rho^2 p(\rho) = \frac{\kappa(\rho/N, \delta_c)}{2\sqrt{2\pi}\sigma_V^2} \exp \left[-\frac{\delta_c^2}{2\sigma_V^2} \kappa^2(\rho/N, \delta_c) \right], \quad (\text{A5})$$

where

$$\kappa(\rho, \delta_c) = \rho^{1/2\delta_c} + \rho^{-1/2\delta_c}. \quad (\text{A6})$$

Setting $\delta_c = 5/3$ means $n = -6/5$ and so

$$N = \frac{5}{3} \frac{e^{25/9\sigma_V^2}}{\sqrt{2\pi}\sigma_V} \left[K_{7/6} \left(\frac{25}{9\sigma_V^2} \right) + K_{13/6} \left(\frac{25}{9\sigma_V^2} \right) \right], \quad (\text{A7})$$

where $K_\nu(x)$ is a modified Bessel function of the second kind. The random walk prediction for this model is

$$\rho^2 p(\rho) = \frac{(\rho/N)^{3/10}}{\sqrt{2\pi}\sigma_V^2} \exp \left[-\frac{25}{18\sigma_V^2} \kappa^2(\rho/N, \delta_c) \right] \quad (\text{A8})$$